Isoindigo-Based Polymers with Small Effective Masses for High-Mobility Ambipolar Field-Effect Transistors

Jie Yang, Zhiyuan Zhao, Hua Geng, Changli Cheng, Jinyang Chen, Yunlong Sun, Longxian Shi, Yuanping Yi, Zhigang Shuai, Yunlong Guo, Shuai Wang,* and Yunqi Liu**

So far, most of the reported high-mobility conjugated polymers are p-type semiconductors. By contrast, the advances in high-mobility ambipolar polymers fall greatly behind those of p-type counterparts. Instead of unipolar p-type and n-type materials, ambipolar polymers, especially balanced ambipolar polymers, are potentially serviceable for easy-fabrication and low-cost complementary metal-oxide-semiconductor circuits. Therefore, it is a critical issue to develop high-mobility ambipolar polymers. Here, three isoindigo-based polymers, PIID-2FBT, P1FIID-2FBT, and P2FIID-2FBT are developed for high-performance ambipolar organic field-effect transistors. After the incorporation of fluorine atoms, the polymers exhibit enhanced coplanarity, lower energy levels, higher crystallinity, and thus increased μ_e. P2FIID-2FBT exhibits n-type dominant performance with a μ_e of 9.70 cm^2 V^{-1} s^{-1}. Moreover, P1FIID-2FBT exhibits a highly balanced μ_h and μ_e of 6.41 and 6.76 cm^2 V^{-1} s^{-1}, respectively, which are among the highest values for balanced ambipolar polymers. Moreover, a concept "effective mass" is introduced to further study the reasons for the high performance of the polymers. All the polymers have small effective masses, indicating good intramolecular charge transport. The results demonstrate that high-mobility ambipolar semiconductors can be obtained by designing polymers with fine-tuned energy levels, small effective masses, and high crystallinity.

Organic field-effect transistors (OFETs) based on polymeric semiconductors offer unique attractions including mechanical flexibility, light weight, solution processability, and low cost compared to traditional silicon-based electronics.[1–4] Recently, donor–acceptor (D–A) conjugated polymers have emerged as excellent candidates for OFETs.[5–7] Especially, D–A polymers based on diketopyrrolopyrrole (**DPP**), isoindigo (**IID**), and naphthalenediimide (**NDI**) exhibit excellent hole-transporting (p-type) or electron-transporting (n-type) characteristics.[8–12] Both p-type and n-type polymeric materials are very necessary for OFET devices to fabricate complementary metal-oxide-semiconductor (CMOS) circuits with low-energy consumption. To date, an ultrahigh hole mobility (μ_h) of 17.8 cm^2 V^{-1} s^{-1} has been achieved by a **DPP**-based polymer.[13] On the other hand, unipolar n-type polymers with electron mobilities (μ_e) of more than 5.0 cm^2 V^{-1} s^{-1} have been successively reported.[14,15] Instead of unipolar p-type and n-type materials, ambipolar polymers, especially balanced ambipolar polymers, which can transport both electrons and holes at the same time, are potentially serviceable for easy-fabrication and low-cost CMOS circuits.[16,17] However, it remains a challenge to obtain high-performance balanced ambipolar polymers.

For high-mobility balanced ambipolar polymers, in general, it is essential to possess an efficient charge (hole or electron) injection from gold electrodes to semiconductors and good charge transport in semiconductors.[18,19] Charge injection can be evaluated by frontier molecular orbital (FMO) energy levels, including the highest occupied molecular orbital (HOMO) and lowest unoccupied molecular orbital (LUMO) energy levels. By selecting suitable acceptors and donors, we can develop polymers with fine-tuned FMO energy levels for an efficient charge injection. For polymeric materials, charge transport includes intramolecular charge transport along the conjugated backbone and intermolecular charge hopping through π–π stacking.

J. Yang, Prof. S. Wang
School of Chemistry and Chemical Engineering
Huazhong University of Science and Technology
Wuhan 430074, P. R. China
E-mail: chmsamuel@hust.edu.cn

J. Yang, Dr. Z. Zhao, J. Chen, Y. Sun, L. Shi,
Prof. Y. Yi, Prof. Y. Guo, Prof. Y. Liu
Beijing National Laboratory for Molecular Sciences
Key Laboratory of Organic Solids
Institute of Chemistry
Chinese Academy of Sciences
Beijing 100190, P. R. China
E-mail: guoyunlong@iccas.ac.cn; liuyq@iccas.ac.cn

Dr. H. Geng
Department of Chemistry
Capital Normal University
Beijing 100048, P. R. China

Dr. C. Cheng, Prof. Z. Shuai
MOE Key Laboratory of Organic OptoElectronics
and Molecular Engineering
Department of Chemistry
Tsinghua University
Beijing 100084, P. R. China

DOI: 10.1002/adma.201702115

Charge transport is influenced by several factors such as molecular weights, main-chain π-conjugation, coplanarity, and crystallinity.[20–24] To obtain fine-tuned FMO energy levels as well as good charge transport, fluorine (F) substitution of a polymeric backbone may be a promising strategy.[14,19,25–35] Among the electron-withdrawing groups, F atom has the highest Pauling electronegativity (4.0) and smallest atom size (van der Waals radius, $r = 1.35$ Å, only slightly larger than hydrogen, $r = 1.2$ Å) which will not cause too much steric hindrance to the intermolecular packing of F-substituted polymers.[27,29] Because of the strong electronegativity of F atom, F substitution lowers not only the HOMO energy level of the polymer, enhancing the oxidative stability, but also the LUMO energy level, facilitating easier electron injection from the electrodes.[25,27] Furthermore, the intramolecular and intermolecular F H or F S noncovalent interactions[14,25–27,31,33] may promote better molecular organization and crystallization to enhance the mobility. Moreover, the hydrophobicity of F-substituted polymers can prevent the diffusion of moisture and oxygen into the films, thus improving the stability of OFET devices in ambient air.[25,27] However, polymers with excess substituted F atoms are generally less soluble[36] and easily preaggregative,[37,38] which is unfavorable for top-gate device characterization. In addition, excess substituted F atoms may cause too low-lying HOMO energy levels or repulsive F···F interactions, which will fairly decrease the μ_h[15,32] or lead to twisted packing.[39,40] Therefore, the numbers of substituted F atoms should be carefully designed in order to obtain high-performance balanced ambipolar polymers. For instance, a recent study by Geng and co-workers[32] reported a F-substituted polymer with μ_h/μ_e of 3.94/3.50 $cm^2\ V^{-1}\ s^{-1}$ based on (*E*)-1,2-bis(3,4-difluorothien-2-yl)ethane (**4FTVT**). However, the reasons for the high mobilities of this polymer were not clear enough, and further studies were required.

Recently, several polymers based on 3,3′-difluoro-2,2′-bithiophene (**2FBT**) donor have been demonstrated to show excellent performances for organic photovoltaic devices.[29,31,41,42] However, there has been little attempt to investigate their OFET performances.[43] It is worth noting that this donor is different from that reported by Geng and co-workers.[32] Here, three **2FBT**-based polymers **PnFIID-2FBT** ($n = 0$–2) containing 0, 1, and 2 F atoms in the acceptor units, were carefully designed to investigate their OFET performances.[44] Due to the simple modulation of numbers and position of substituted F atoms, isoindigo was selected as the acceptor, which was also used in other work.[26,45] After the incorporation of F atoms, the polymers showed enhanced coplanarity, lower FMOs, and higher crystallinity. As a result, **PIID-2FBT** exhibited p-type dominant performance with μ_h and μ_e of 5.33 and 2.06 $cm^2\ V^{-1}\ s^{-1}$, respectively. Balanced ambipolar **P1FIID-2FBT** with μ_h/μ_e of 6.41/6.76 $cm^2\ V^{-1}\ s^{-1}$, and n-type dominant **P2FIID-2FBT** with μ_h/μ_e of 2.75/9.70 $cm^2\ V^{-1}\ s^{-1}$ were achieved. Compared to reports in the literature, **P1FIID-2FBT** achieved the record mobility values for balanced ambipolar polymers.[18,19] To elucidate the reasons for the high mobilities of these polymers, we performed theoretical calculations on the effective masses (m^*) of charges, which can be related to the ability of charge transport in semiconductors.[46] Note that **P2FIID-2FBT** showed a relatively small m_e^* (m^* of electrons) of 0.116 m_e (the mass of an electron), consistent with the high μ_e.

Scheme 1 presents the synthetic route to **PnFIID-2FBT**. Novel routes to the monomers **1FIID** and **2FIID** were developed (Figures S6 and S7, Supporting Information). The synthetic details are provided in the Supporting Information. 6-Bromo-7-fluoroisatin (**3**) and *N*-alkylated isoindigo (**IID**) were synthesized according to the literature.[25] The alkylation of 6-bromoisatin (**1**) or compound **3** gave compound **2** or **4**, respectively. Compound **4** was reduced by hydrazine monohydrate, in 1,4-dioxane solution, to afford compound **5**. The monomer **1FIID** or **2FIID** was readily obtained by a condensation reaction between compound **2** or **4** and compound **5**, respectively, in acidic medium. Stille coupling polymerization among **IID**, **1FIID**, or **2FIID** and 5,5′-bis(trimethylstannyl)-3,3′-difluoro-2,2′-bithiophene afforded the corresponding polymer. Due to the asymmetric structure of **1FIID** and lack of selectivity of the reaction between **1FIID** and stannylated species, the polymer **P1FIID-2FBT** had several possible molecular structures (Figure S1, Supporting Information).[47–49] Previous studies have shown that polymers composed of centrosymmetrical acceptors and donors exhibited higher mobilities due to their better intermolecular packing.[50] Although **P1FIID-2FBT** is composed of unsymmetrical acceptors, its intermolecular packing may not be obviously disturbed due to the comparable atom sizes of F and H atoms as discussed above. So **P1FIID-2FBT** may show high performance. After purification by Soxhlet extraction, all the polymers were completely extracted into chlorobenzene. The molecular weights of **PnFIID-2FBT** were determined by high-temperature gel permeation chromatography (GPC) at 150 °C using 1,2,4-tricholorobenzene as the eluent (Figure S8, Supporting Information). **PIID-2FBT**, **P1FIID-2FBT**, and **P2FIID-2FBT** displayed high molecular weights with M_n of 57.1, 50.5, and 59.0 kDa, respectively. Thermogravimetric analysis curves indicated that all the polymers exhibited excellent thermal stability with decomposition temperatures over 400 °C (Figure S9, Supporting Information).

The optical properties of the polymers were investigated by UV–vis absorption spectra (Figure S10, Supporting Information). All the polymers exhibited typically dual absorption bands (Bands I and II) in chlorobenzene solution and in thin film.[25,51] Figure S2 (Supporting Information) shows the simulated UV–vis absorption spectra calculated by time-dependent-density functional theory (DFT) calculations, which can be used to assign the experimental absorption peaks.[32,35] Absorption bands ranging from 300 to 500 nm (Band II) were ascribed to the π–π* (HOMO → LUMO + 1) transitions, while broad absorption bands extending from 600 to 900 nm (Band I) mainly originated from the intramolecular charge transfer. We observed that obvious red shifts of Band I and slight blue shifts of Band II occurred in going **PIID-2FBT** to **P2FIID-2FBT**, especially in solution (Figure S10a, Supporting Information). The maximum absorption peak of **PIID-2FBT** in film (720 nm) exhibited a slight red shift compared to that in solution (711 nm). This phenomenon was also observed for **P1FIID-2FBT** and **P2FIID-2FBT**, indicating the planarization of the polymer backbones in the solid state (Table S1, Supporting Information). The optical bandgap of **P2FIID-2FBT** (1.40 eV) calculated from the onset of absorption in the spectrum of the thin film was obviously narrower than that of **PIID-2FBT** (1.54 eV) or **P1FIID-2FBT** (1.57 eV) (Table S1, Supporting

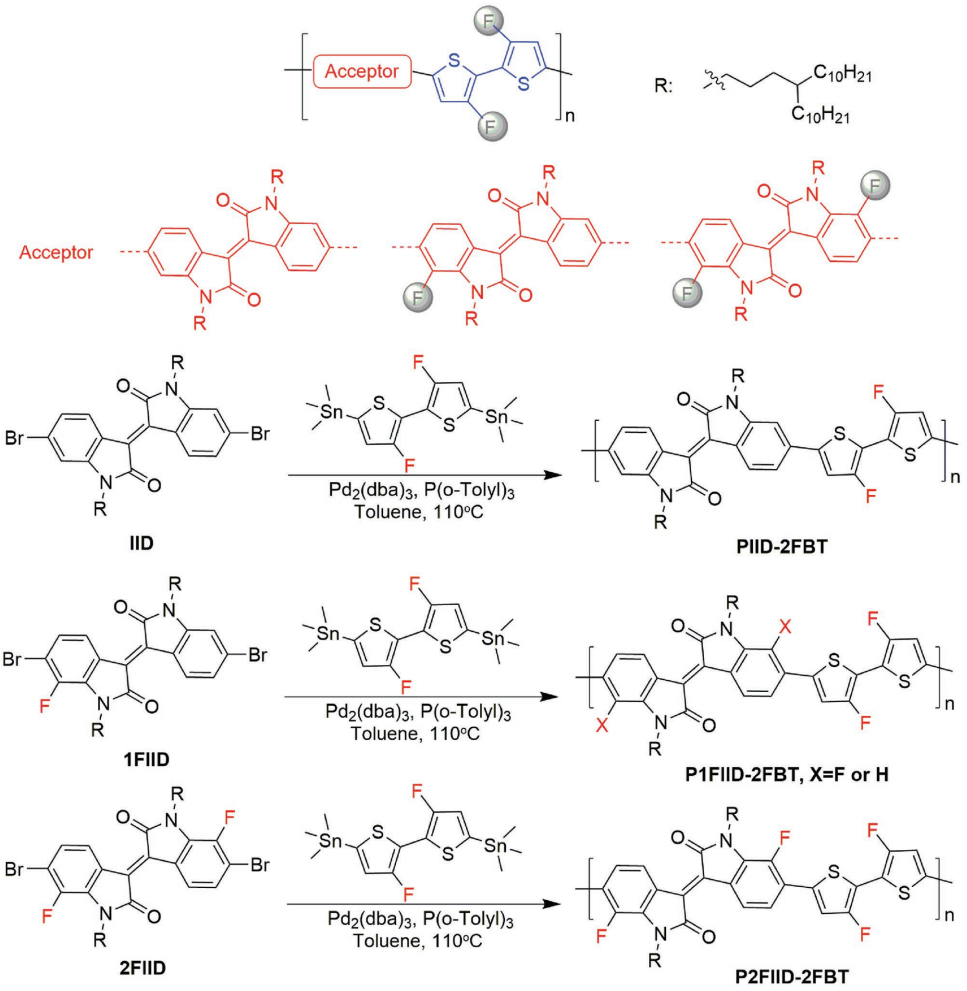

Scheme 1. Molecular structures of **2FBT**-based polymers and their synthetic routes. "Acceptor" represents **IID**, **1FIID**, and **2FIID**, respectively.

Information), which was ascribed to the enhanced coplanarity of **P2FIID-2FBT**.

The electrochemical properties of the polymers were investigated by cyclic voltammetry (CV) (Figure S11, Supporting Information). Notably, all the polymers exhibited intense oxidation and reduction peaks, suggesting that they could act as ambipolar semiconductors. The FMO energy levels of the three polymers were calculated from the onsets of oxidation and reduction using the equation $E = -(E_{onset} + 4.40\ eV)$. The calculated HOMO energy levels were −5.66 eV for **PIID-2FBT**, −5.63 eV for **P1FIID-2FBT**, and −5.72 eV for **P2FIID-2FBT**, respectively (Table S1, Supporting Information). By contrast, after the incorporation of F atoms, the LUMO energy levels of the polymers were significantly lowered in going from **PIID-2FBT** to **P2FIID-2FBT**. The LUMO energy level of **P2FIID-2FBT** reached −3.64 eV, lower than those of **P1FIID-2FBT** (−3.55 eV) and **PIID-2FBT** (−3.46 eV). The effect of F substitution on the FMO energy levels was also investigated by DFT calculations. Figure S3 (Supporting Information) shows the calculated FMO energy levels for the oligomers (n = 1–4) and polymers ($n = \infty$) of **PnFIID-2FBT**. F substitution lowered both the HOMO and LUMO energy levels but only obvious decreases (from −3.26 to −3.46 eV) were found for the LUMO energy levels. Therefore, the trend of the FMO energy levels in the experiments was consistent with the theoretical data (Table S1, Supporting Information).

The crystalline natures and film morphologies of the polymers were studied by 2D grazing incident X-ray diffraction (2D-GIXRD) and atomic force microscopy (AFM). The 2D-GIXRD patterns of the as-spun and 180 °C annealed films are shown in **Figure 1**. For the as-spun films of all the polymers, (h00) diffraction peaks up to fourth order were observed along the out-of-plane (q_z) direction (Figure S12a–c, Supporting Information). After thermal annealing at 180 °C, the (h00) diffraction peaks became sharper and stronger, indicating significantly enhanced crystallinity of the films. Different from the as-spun films of **PIID-2FBT** and **P1FIID-2FBT**, the (010) diffraction, attributed to π–π stacking, was visible for **P2FIID-2FBT**, indicating a strong crystalline tendency caused by a multitude of F atoms. **PIID-2FBT**, **P1FIID-2FBT**, and **P2FIID-2FBT** displayed lamellar d-spacing of 24.52, 23.59, and 25.03 Å, respectively, corresponding to out-of-plane (100) diffractions (Figure S12d–f, Supporting Information). All the polymers exhibited bimodal distributions of face-on and edge-on crystallites, as evidenced by the observation of the (010) diffraction peaks along both the in-plane (q_{xy}) and out-of-plane directions. Notably, the

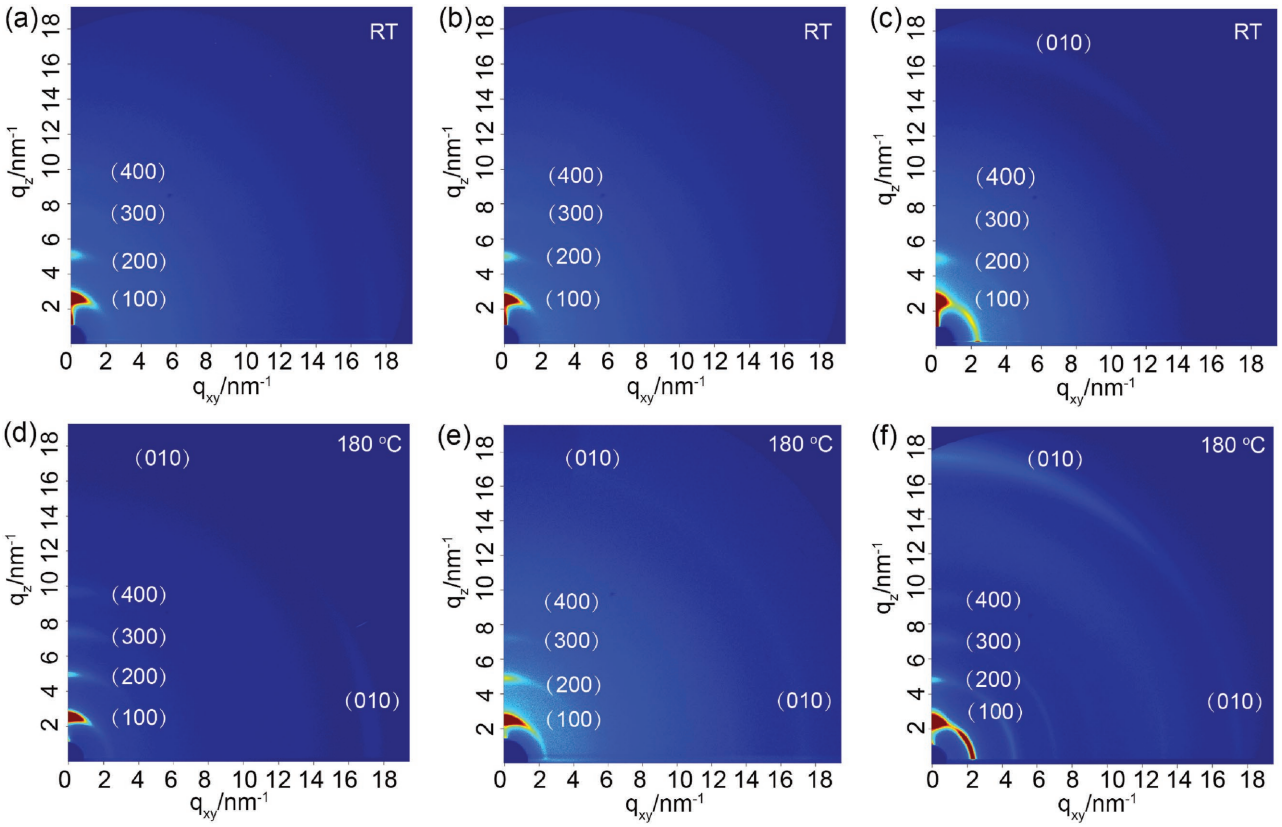

Figure 1. 2D-GIXRD patterns of a) as-spun and d) annealed **PIID-2FBT** films; b) as-spun and e) annealed **P1FIID-2FBT** films; c) as-spun and f) annealed **P2FIID-2FBT** films.

annealing process caused the orientation of **P2FIID-2FBT** film to achieve bimodal distribution from face-on feature as the (010) diffraction peak only existed along the out-of-plane direction for the as-spun film (Figure 1c,f). According to the in-plane (010) diffraction peaks, **PIID-2FBT**, **P1FIID-2FBT**, and **P2FIID-2FBT** displayed successively closer π–π distances of 3.55, 3.52, and 3.50 Å, respectively (Figure S12d–f, Supporting Information), resulting from the enhanced coplanarity and stronger intermolecular interactions.[14] The lamellar and π–π stacking crystalline correlation lengths (CCL) of the polymers were calculated using the Scherrer's equation (Table S2, Supporting Information).[23,52] The π–π stacking CCLs of **PIID-2FBT**, **P1FIID-2FBT**, and **P2FIID-2FBT** calculated from the (010) diffractions were 5.8, 7.0, and 7.5 nm, respectively. CCL is related to both the number of scattering lattice plains and the degree of crystalline order in a crystallite.[14] Better crystallinity results in a larger CCL. Figure S13 (Supporting Information) presents the AFM images of polymeric films deposited on octadecyltrichlorosilane (OTS)-modified SiO_2 substrates after annealing at 180 °C. As the AFM morphologies revealed, all the polymeric films showed well-interconnected large domains which could minimize the intergranular charge hopping barriers.[32,53] **PIID-2FBT** and **P1FIID-2FBT** displayed granular morphologies, whereas **P2FIID-2FBT** showed more uniform fiber-like polycrystalline grains. In going from **PIID-2FBT** to **P2FIID-2FBT**, the polymers showed larger polycrystalline grains together with increased root-mean-square (RMS) roughness, consistent with larger CCLs. Overall, from **PIID-2FBT** to **P2FIID-2FBT**, the closer π–π distances, increased π–π stacking CCLs, and larger polycrystalline grains suggested that F substitution could improve the crystallinity of the polymers, which was favorable for improving intermolecular charge hopping.

OFETs with a top-gate bottom-contact (TGBC) architecture were fabricated to investigate the carrier transport properties of the three polymers. This device configuration was preferentially used for ambipolar or n-type semiconducting polymers due to its encapsulation effect of the top dielectric layer.[25] High-molecular-weight polymethyl methacrylate (PMMA) was used as the dielectric due to a low trap density, which was favorable for a high μ_e.[15,54,55] The semiconducting layers were deposited by spin-coating in a nitrogen glove box and all the OFET devices were measured under ambient conditions. The experimental details for the fabrication of TGBC OFET devices fabrication are provided in the Supporting Information. Figure S14 (Supporting Information) shows the corresponding mobilities of the polymers at different annealing temperatures. The observation of smallest RMS roughness values for all the polymers at 180 °C suggested the smoothest interface (Figures S15–S17, Supporting Information), which was beneficial for charge transport and induced high mobility in top-gate OFETs.[26,56] **Figure 2**a–c and Figures S18–S20 (Supporting Information) provide the typical transfer and output curves of the polymers at the optimal annealing temperature (180 °C), respectively. Hole transport was evaluated from the negative gate sweeping from 0 to –100 V,

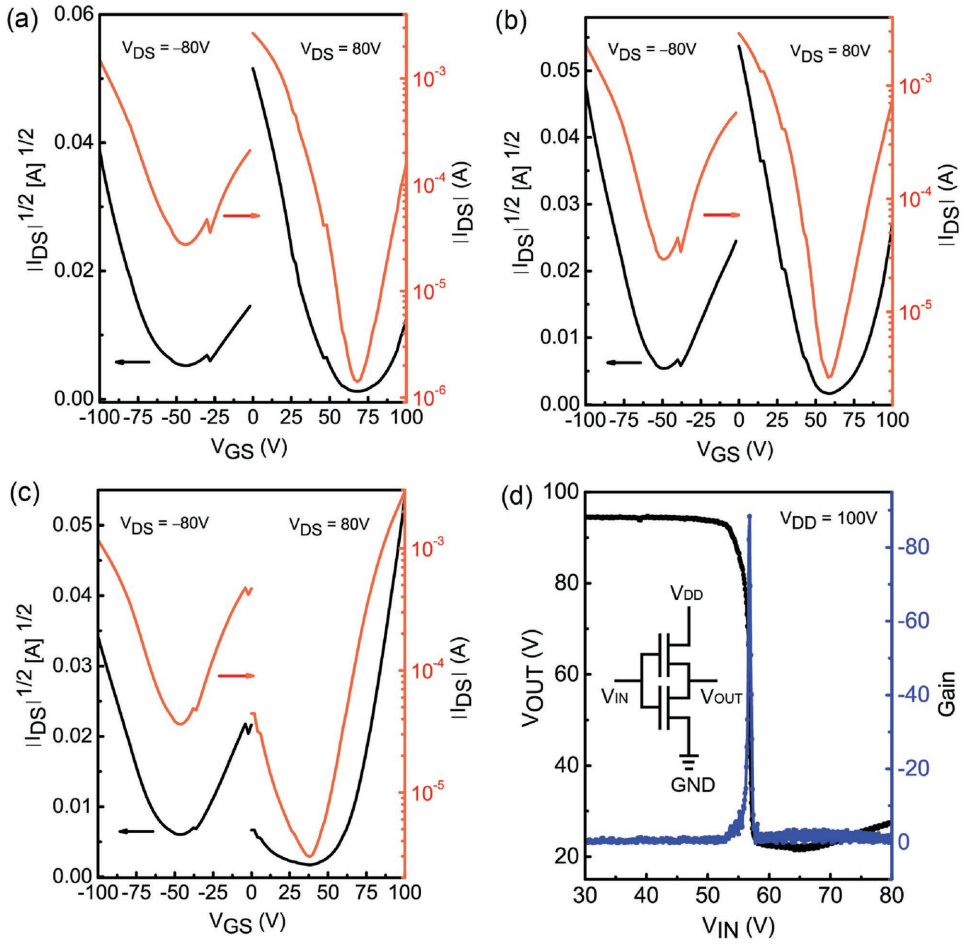

Figure 2. Typical transfer characteristics of TGBC OFETs based on a) **PIID-2FBT**, b) **P1FIID-2FBT**, and c) **P2FIID-2FBT**. d) The transfer characteristic and gain of a complementary-like inverter. The steepness of the inverter curve indicates a gain of 94. (Inset: inverter circuit configuration).

while electron transport from 0 to 100 V. Weak dependences of the μ_h and μ_e on V_G were observed for OFETs fabricated from all the polymers, suggesting an identical carrier mobility beyond the threshold voltage (Figure S21, Supporting Information).

All of the polymers exhibited ambipolar transport behaviors with typical V-shaped transfer curves as shown in Figure 2a–c. The μ_h and μ_e data extracted from the transfer characteristics in the saturation and linear regimes are summarized in **Table 1** and Table S4 (Supporting Information), respectively. After the incorporation of F atoms, the polymers showed obvious mobility changes from p-channel dominant to balanced ambipolar, and n-channel dominant transport characteristics. As shown in Table 1, **PIID-2FBT** exhibited maximum μ_h and μ_e of 5.33 and 2.06 cm^2 V^{-1} s^{-1}, respectively. On the other hand, **P1FIID-2FBT** exhibited perfectly balanced μ_h and μ_e up to 6.41 and 6.76 cm^2 V^{-1} s^{-1}, respectively (μ_h/μ_e = 0.95). Compared to the two polymers discussed above, a decreased μ_h of 2.75 cm^2 V^{-1} s^{-1} and an increased μ_e of 9.70 cm^2 V^{-1} s^{-1} were observed for **P2FIID-2FBT**. To the best of our knowledge, this μ_e is among the highest values for n-type polymers (Table S3, Supporting Information). In going from **PIID-2FBT** to **P2FIID-2FBT**, threshold voltage

Table 1. Effective masses and OFET performances of the three polymers.

Polymer	m_h*/m_e*[a] (m_e)	p-type			n-type		
		μ_h[b] [cm^2 V^{-1} s^{-1}]	V_{th}[c] [V]	I_{on}/I_{off}[d]	μ_e[b] [cm^2 V^{-1} s^{-1}]	V_{th}[c] [V]	I_{on}/I_{off}[d]
PIID-2FBT	0.102/0.121	5.33 (4.87)	−57 (±4)	10–10^2	2.06 (1.82)	77 (±5)	10^2–10^3
P1FIID-2FBT	0.099/0.118	6.41 (5.88)	−56 (±4)	10–10^2	6.76 (6.12)	75 (±4)	10^2–10^3
P2FIID-2FBT	0.097/0.116	2.75 (2.25)	−57 (±2)	10–10^2	9.70 (9.16)	57 (±4)	10^3–10^4

[a]Hole and electron effective masses (m_h* and m_e*) obtained from the theoretical calculations. Here m_e represents the mass of an electron; [b]Maximum mobilities extracted from the transfer curves in the saturation regimes. The average values are listed in parentheses; [c]Threshold voltage; [d]On–off current ratio.

(V_{th}) values decreased for n-channel but no clear trend was found for p-channel. The OFET devices were stored under ambient conditions to investigate their air stability. As shown in Figure S22 (Supporting Information), no obvious degradations were observed for hole and electron mobilities of the three polymers in 90 d due to the encapsulation effect of the thick PMMA (1350 nm) dielectric layers, which could significantly reduce the negative influence from water or oxygen in air.[15] The well-balanced ambipolar nature of **P1FIID-2FBT** prompted us to fabricate CMOS-like inverters using two identical ambipolar OFETs based on one-component polymer (**P1FIID-2FBT**). The detailed fabrication procedures are provided in the Supporting Information. As shown in Figure 2d, the maximum gain of the inverters was about 94, which is among the highest values reported for inverters based on single-components.[16,56–58]

The effect of F substitution on charge transport (intramolecular charge transport along the conjugated backbone and intermolecular charge hopping through π–π stacking) in the polymers was examined by theoretical calculations (**Figure 3**). It is known that intramolecular charge transport is influenced by the intrinsic molecular structure including π-conjugation, coplanarity, electron deficiency, etc. Although intramolecular charge transport plays an important role in high-mobility polymers, it is difficult to evaluate by experimental methods.[21,23] Here, we introduce the concept "m^*" to evaluate intramolecular charge transport of polymers, where a small m^* reveals efficient intramolecular charge transport. Recently, our group demonstrated the calculation of m^* based on the novel super-exchange (Figure S4, Supporting Information) model and first-principle computations from the perspective of theoretical calculations.[46] Based on above computational methods, the m^* of the three polymers was calculated (Figure 3c–f).[46] Figure 3d–f shows the calculated band structures and densities of states (DOS). A quasi mirror symmetry between the conduction and valence bands along polymer backbone direction was observed (Figure 3d–f). This result indicated that the electronic couplings (transfer integral) for holes and electrons were very similar. Based on the second derivative of band structure, m_h^* (m^* of holes) and m_e^* were calculated respectively. As shown in Table 1, all the polymers showed relatively small m_h^* and m_e^*. In going from **PIID-2FBT** to **P2FIID-2FBT**, the m_h^* and m_e^* decreased simultaneously (Figure 3c). Thus, the intramolecular charge transport in **P2FIID-2FBT** was the most efficient. **P2FIID-2FBT** showed a m_h^* and m_e^* of 0.097 m_e and 0.116 m_e, respectively. These

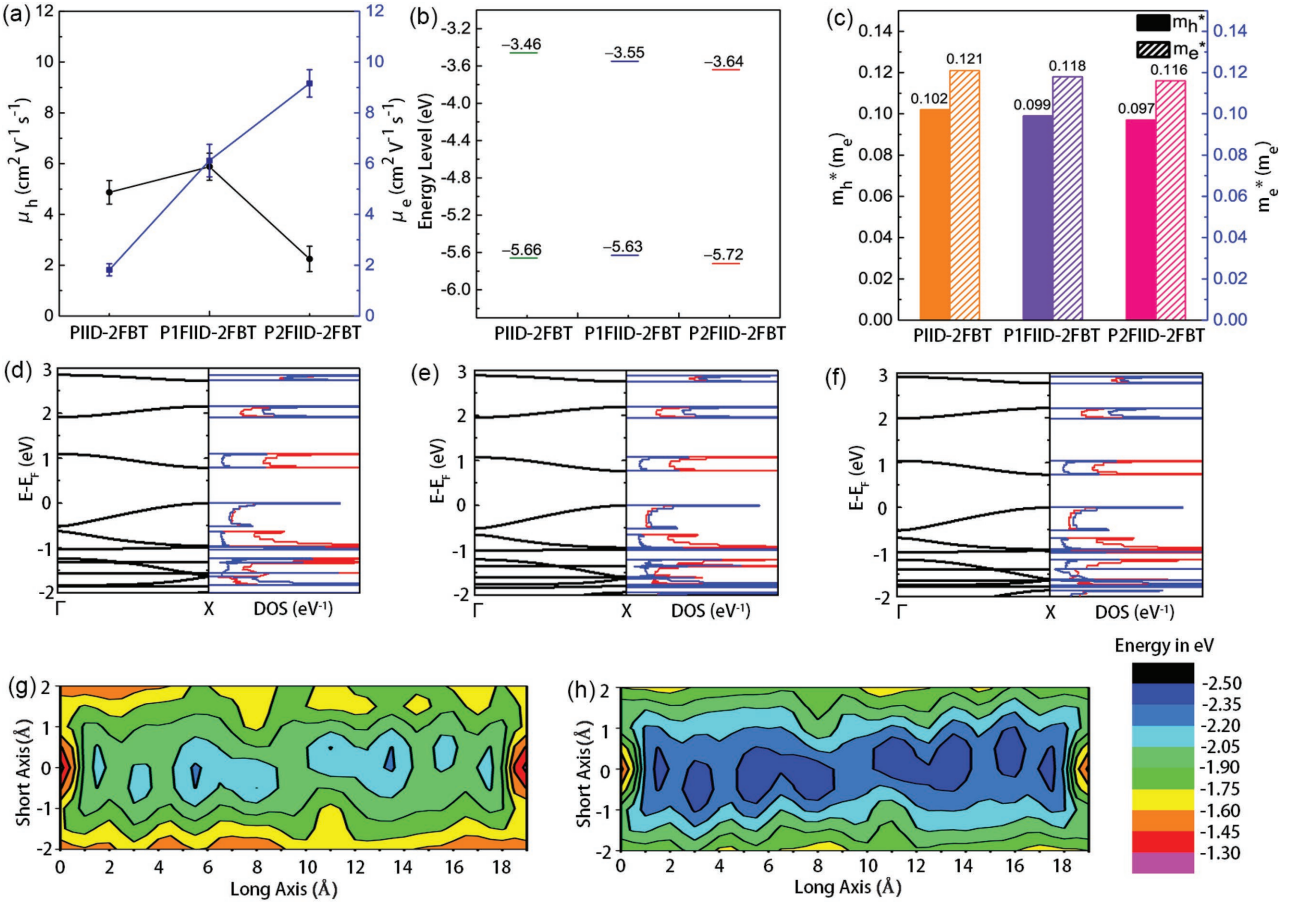

Figure 3. a) Hole and electron mobilities of the three polymers extracted from the transfer curves. b) HOMO and LUMO energy levels of the three polymers determined from CV. c) Hole and electron effective masses (m_h^* and m_e^*) obtained from the theoretical calculations. Band structures and partial densities of states (DOS) of d) **PIID-2FBT**, e) **P1FIID-2FBT**, and f) **P2FIID-2FBT**. Red lines represent the contributions from acceptors, while blue lines represent the contributions from donors. Contour plots for intermolecular binding energy of g) **PIID-2FBT** and h) **P2FIID-2FBT** in the plane of the backbone.

values are comparable to those of cyclopentadithiophene-pyridinethiadiazole (m_h* = 0.106 m_e), which could achieve a high μ_h up to 47 cm^2 V^{-1} s^{-1}.[59,60] In order to gain insight into intermolecular stacking information, the total energy of lattice was calculated as a function of intermolecular relative displacement. For simplicity, only **PIID-2FBT** and **P2FIID-2FBT** were used as models. The contour plots for intermolecular binding energy are shown in Figure 3g,h and Figure S5 (Supporting Information). Geometry-optimized isolated chain and π–π stacking distance from the XRD data were adopted at M06-2X/6-31G(d) level with CRYSTAL14 code.[61] **P2FIID-2FBT** exhibited a much smaller binding energy than that of **PIID-2FBT**, indicating that F substitution increased electrostatic interaction and thus induced close stacking, which was convenient for 2D intermolecular charge hopping. These theoretical data were consistent with 2D-GIXRD and AFM results. Therefore, F substitution of the polymers can achieve more effective intramolecular charge transport as well as intermolecular charge hopping.

PIID-2FBT and **P1FIID-2FBT** exhibited close μ_h, superior to that of **P2FIID-2FBT**. In comparison, the μ_e showed successive increase in going from **PIID-2FBT** to **P2FIID-2FBT** (Figure 3a). Based on the above CV, GIXRD, AFM, and theoretical data, we tried to illustrate the trend of the μ_h and μ_e of the three polymers from the aspects of charge injection and charge transport. F substitution promoted both better hole and electron transport resulting from the smaller m_h* and m_e* (Figure 3c) and better crystallinity (GIXRD data) of the polymers in going from **PIID-2FBT** to **P2FIID-2FBT**. According to the gold work function (4.7–5.2 eV), the electron injection from the electrode to the polymers was gradually improved in going from **PIID-2FBT** (LUMO = −3.46 eV) to **P2FIID-2FBT** (LUMO = −3.64 eV) (Figure 3b). Therefore, the increase in μ_e from 2.06 to 9.70 cm^2 V^{-1} s^{-1} was the combined result of more efficient electron injection (lower LUMO) and better electron transport (smaller m_e* and better crystallinity). Compared to **PIID-2FBT** and **P1FIID-2FBT**, however, **P2FIID-2FBT** exhibited the largest injection barrier between the HOMO energy level (–5.72 eV) and gold work function, leading to the worst hole injection. Therefore, the relatively inferior μ_h (2.75 cm^2 V^{-1} s^{-1}) of **P2FIID-2FBT** should be mainly ascribed to hindered hole injection although it exhibited efficient hole transport.

In conclusion, three **2FBT**-based polymers **PIID-2FBT**, **P1FIID-2FBT**, and **P2FIID-2FBT** were developed for high-performance ambipolar OFETs. In going from **PIID-2FBT** to **P2FIID-2FBT**, the polymers exhibited enhanced coplanarity, lower FMOs, higher crystallinity, and thus increased μ_e. **P2FIID-2FBT** exhibited n-type dominant performance with a μ_e of 9.70 cm^2 V^{-1} s^{-1}. Moreover, **P1FIID-2FBT** exhibited balanced μ_h and μ_e of 6.41 and 6.76 cm^2 V^{-1} s^{-1}, respectively, which are among the highest values for balanced ambipolar polymers. The concept "*m**" was introduced to further study the reasons for the high performance of the polymers. All the 2FBT-based polymers had small *m**, indicating good intramolecular charge transport. Therefore, **2FBT** is a promising donor to obtain high-performance ambipolar polymers. The results have demonstrated that high-mobility ambipolar semiconductors can be obtained by designing polymers with fine-tuned energy levels, small *m**, and high crystallinity.

Experimental Section

Synthesis of ***PIID-2FBT***: **IID** (100.0 mg, 0.0915 mmol), 5,5′-bis(trimethylstannyl)-3,3′-difluoro-2,2′-bithiophene (48.3 mg, 0.0915 mmol), $Pd_2(dba)_3$ (2.5 mg), P(*o*-tol)$_3$ (6.7 mg), and toluene (5 mL) were added to a Schlenk tube. The tube was charged with argon through a freeze-pump-thaw cycle for three times. The mixture was stirred for 10 min at 110 °C, cooled down to room temperature, and poured into methanol (100 mL) containing hydrochloric acid (5 mL) and stirred for 3 h. The precipitated product was filtered and purified via Soxhlet extraction with methanol (10 h), acetone (10 h), hexane (10 h), chloroform (10 h), and was finally collected with chlorobenzene. The chlorobenzene fraction was concentrated by evaporation and precipitated into methanol (100 mL) and filtered off to afford the target polymer (82 mg, 79.1%). GPC: M_n = 57.1 kDa, M_w = 166.8 kDa, PDI = 2.92. Anal. calcd. for $C_{72}H_{106}F_2N_2O_2S_2$: C 76.27, H 9.42, N 2.47; found: C 76.07, H 9.42 , N 2.65.

Synthesis of ***P1FIID-2FBT***: The synthetic procedure is similar as described for **PIID-2FBT** (86 mg, 80.1%). GPC: M_n = 50.5 kDa, M_w = 137.5 kDa, PDI = 2.72. Anal. calcd. for $C_{72}H_{105}F_3N_2O_2S_2$: C 75.08, H 9.19, N 2.43; found: C 74.83, H 9.29, N 2.61.

Synthesis of ***P2FIID-2FBT***: The synthetic procedure is similar as described for **PIID-2FBT** (80 mg, 77.2%). GPC: M_n = 59.0 kDa, M_w = 146.1 kDa, PDI = 2.48. Anal. calcd. for $C_{72}H_{104}F_4N_2O_2S_2$: C 73.93, H 8.96, N 2.39; found: C 73.49, H 8.92, N 2.35.

Supporting Information

Supporting Information is available from the Wiley Online Library or from the author.

Acknowledgements

J.Y., Z.Z., and H.G. contributed equally to this work. This work was financially supported by the National Key R&D Program of "Strategic Adanced Electronic Materials" (No. 2016YFB0401100), the National Natural Science Foundation of China (Grant Numbers: 21673247, 51233006, and 21633012), the Major State Basic Research Development Program (2013CB733700), and the Strategic Priority Research Program of the Chinese Academy of Sciences (No. XDB12030100). 2D-GIXRD results were obtained at 1W1A Station of Beijing Synchrotron Radiation Facility. The authors gratefully acknowledge the assistance of scientists of the Diffuse X-ray Scattering Station during the experiments.

Conflict of Interest

The authors declare no conflict of interest.

Keywords

ambipolar, effective mass, fluorosubstitution, high mobility, field-effect transistors

Received: April 15, 2017
Revised: June 22, 2017
Published online: July 24, 2017

[1] H. Yan, Z. Chen, Y. Zheng, C. Newman, J. R. Quinn, F. Dotz, M. Kastler, A. Facchetti, *Nature* **2009**, *457*, 679.
[2] A. C. Arias, J. D. MacKenzie, I. McCulloch, J. Rivnay, A. Salleo, *Chem. Rev.* **2010**, *110*, 3.

[3] H. Sirringhaus, *Adv. Mater.* **2014**, *26*, 1319.
[4] J. Y. Oh, S. Rondeau-Gagné, Y.-C. Chiu, A. Chortos, F. Lissel, G.-J. N. Wang, B. C. Schroeder, T. Kurosawa, J. Lopez, T. Katsumata, J. Xu, C. Zhu, X. Gu, W.-G. Bae, Y. Kim, L. Jin, J. W. Chung, J. B. H. Tok, Z. Bao, *Nature* **2016**, *539*, 411.
[5] C. Wang, H. Dong, W. Hu, Y. Liu, D. Zhu, *Chem. Rev.* **2012**, *112*, 2208.
[6] J. D. Yuen, F. Wudl, *Energy Environ. Sci.* **2013**, *6*, 392.
[7] X. Guo, A. Facchetti, T. J. Marks, *Chem. Rev.* **2014**, *114*, 8943.
[8] Z. Yi, S. Wang, Y. Liu, *Adv. Mater.* **2015**, *27*, 3589.
[9] T. Lei, J.-Y. Wang, J. Pei, *Acc. Chem. Res.* **2014**, *47*, 1117.
[10] E. Wang, W. Mammo, M. R. Andersson, *Adv. Mater.* **2014**, *26*, 1801.
[11] N. Sakai, J. Mareda, E. Vauthey, S. Matile, *Chem. Commun.* **2010**, *46*, 4225.
[12] S.-L. Suraru, F. Würthner, *Angew. Chem., Int. Ed.* **2014**, *53*, 7428.
[13] J. Y. Back, H. Yu, I. Song, I. Kang, H. Ahn, T. J. Shin, S.-K. Kwon, J. H. Oh, Y.-H. Kim, *Chem. Mater.* **2015**, *27*, 1732.
[14] Y.-Q. Zheng, T. Lei, J.-H. Dou, X. Xia, J.-Y. Wang, C.-J. Liu, J. Pei, *Adv. Mater.* **2016**, *28*, 7213.
[15] Z. Zhao, Z. Yin, H. Chen, L. Zheng, C. Zhu, L. Zhang, S. Tan, H. Wang, Y. Guo, Q. Tang, Y. Liu, *Adv. Mater.* **2017**, *29*, 1602410.
[16] J. D. Yuen, R. Kumar, D. Zakhidov, J. Seifter, B. Lim, A. J. Heeger, F. Wudl, *Adv. Mater.* **2011**, *23*, 3780.
[17] K.-J. Baeg, M. Caironi, Y.-Y. Noh, *Adv. Mater.* **2013**, *25*, 4210.
[18] J. Lee, A. R. Han, H. Yu, T. J. Shin, C. Yang, J. H. Oh, *J. Am. Chem. Soc.* **2013**, *135*, 9540.
[19] Y. Gao, X. Zhang, H. Tian, J. Zhang, D. Yan, Y. Geng, F. Wang, *Adv. Mater.* **2015**, *27*, 6753.
[20] R. Noriega, J. Rivnay, K. Vandewal, F. P. V. Koch, N. Stingelin, P. Smith, M. F. Toney, A. Salleo, *Nat. Mater.* **2013**, *12*, 1038.
[21] X. Zhang, H. Bronstein, A. J. Kronemeijer, J. Smith, Y. Kim, R. J. Kline, L. J. Richter, T. D. Anthopoulos, H. Sirringhaus, K. Song, M. Heeney, W. Zhang, I. McCulloch, D. M. DeLongchamp, *Nat. Commun.* **2013**, *4*, 2238.
[22] D. Venkateshvaran, M. Nikolka, A. Sadhanala, V. Lemaur, M. Zelazny, M. Kepa, M. Hurhangee, A. J. Kronemeijer, V. Pecunia, I. Nasrallah, I. Romanov, K. Broch, I. McCulloch, D. Emin, Y. Olivier, J. Cornil, D. Beljonne, H. Sirringhaus, *Nature* **2014**, *515*, 384.
[23] H.-R. Tseng, H. Phan, C. Luo, M. Wang, L. A. Perez, S. N. Patel, L. Ying, E. J. Kramer, T.-Q. Nguyen, G. C. Bazan, A. J. Heeger, *Adv. Mater.* **2014**, *26*, 2993.
[24] Y. Zhao, X. Zhao, M. Roders, G. Qu, Y. Diao, A. L. Ayzner, J. Mei, *Chem. Mater.* **2015**, *27*, 7164.
[25] T. Lei, J.-H. Dou, Z.-J. Ma, C.-H. Yao, C.-J. Liu, J.-Y. Wang, J. Pei, *J. Am. Chem. Soc.* **2012**, *134*, 20025.
[26] T. Lei, X. Xia, J.-Y. Wang, C.-J. Liu, J. Pei, *J. Am. Chem. Soc.* **2014**, *136*, 2135.
[27] J. H. Park, E. H. Jung, J. W. Jung, W. H. Jo, *Adv. Mater.* **2013**, *25*, 2583.
[28] J.-H. Dou, Y.-Q. Zheng, Z.-F. Yao, Z.-A. Yu, T. Lei, X. Shen, X.-Y. Luo, J. Sun, S.-D. Zhang, Y.-F. Ding, G. Han, Y. Yi, J.-Y. Wang, J. Pei, *J. Am. Chem. Soc.* **2015**, *137*, 15947.
[29] J. W. Jung, J. W. Jo, C.-C. Chueh, F. Liu, W. H. Jo, T. P. Russell, A. K. Y. Jen, *Adv. Mater.* **2015**, *27*, 3310.
[30] C. J. Mueller, C. R. Singh, M. Fried, S. Huettner, M. Thelakkat, *Adv. Funct. Mater.* **2015**, *25*, 3454.
[31] K. Kawashima, T. Fukuhara, Y. Suda, Y. Suzuki, T. Koganezawa, H. Yoshida, H. Ohkita, I. Osaka, K. Takimiya, *J. Am. Chem. Soc.* **2016**, *138*, 10265.
[32] Y. Gao, Y. Deng, H. Tian, J. Zhang, D. Yan, Y. Geng, F. Wang, *Adv. Mater.* **2017**, *29*, 1606217.
[33] B. Kang, R. Kim, S. B. Lee, S.-K. Kwon, Y.-H. Kim, K. Cho, *J. Am. Chem. Soc.* **2016**, *138*, 3679.
[34] S. Park, J. Cho, M. J. Ko, D. S. Chung, H. J. Son, *Macromolecules* **2015**, *48*, 3883.
[35] B. Nketia-Yawson, H.-S. Lee, D. Seo, Y. Yoon, W.-T. Park, K. Kwak, H. J. Son, B. Kim, Y.-Y. Noh, *Adv. Mater.* **2015**, *27*, 3045.
[36] K. Miao, G. J. Chae, X. Wu, Q. Shu, X. Zhu, B. Sun, J. Fan, S. Cho, *RSC Adv.* **2016**, *6*, 29164.
[37] H. Bronstein, J. M. Frost, A. Hadipour, Y. Kim, C. B. Nielsen, R. S. Ashraf, B. P. Rand, S. Watkins, I. McCulloch, *Chem. Mater.* **2013**, *25*, 277.
[38] Z. Chen, P. Cai, J. Chen, X. Liu, L. Zhang, L. Lan, J. Peng, Y. Ma, Y. Cao, *Adv. Mater.* **2014**, *26*, 2586.
[39] R. Schmidt, M. M. Ling, J. H. Oh, M. Winkler, M. Könemann, Z. Bao, F. Würthner, *Adv. Mater.* **2007**, *19*, 3692.
[40] R. Schmidt, J. H. Oh, Y.-S. Sun, M. Deppisch, A.-M. Krause, K. Radacki, H. Braunschweig, M. Könemann, P. Erk, Z. Bao, F. Würthner, *J. Am. Chem. Soc.* **2009**, *131*, 6215.
[41] Z. Zheng, S. Zhang, J. Zhang, Y. Qin, W. Li, R. Yu, Z. Wei, J. Hou, *Adv. Mater.* **2016**, *28*, 5133.
[42] X. Long, Z. Ding, C. Dou, J. Zhang, J. Liu, L. Wang, *Adv. Mater.* **2016**, *28*, 6504.
[43] G. E. Park, S. Choi, J. Shin, M. J. Cho, D. H. Choi, *Org. Electron* **2016**, *34*, 157.
[44] Y. Liu, J. Yang, Z. Zhao, J. Chen, L. Shi, Y. Guo, S. Wang, *China Patent 201611102164.0*, **2016**.
[45] Z. Ma, W. Sun, S. Himmelberger, K. Vandewal, Z. Tang, J. Bergqvist, A. Salleo, J. W. Andreasen, O. Inganas, M. R. Andersson, C. Muller, F. Zhang, E. Wang, *Energy Environ. Sci.* **2014**, *7*, 361.
[46] C. Cheng, H. Geng, Y. Yi, Z. Shuai, *J. Mater. Chem. C* **2017**, *5*, 3247.
[47] H.-J. Yun, S.-J. Kang, Y. Xu, S. O. Kim, Y.-H. Kim, Y.-Y. Noh, S.-K. Kwon, *Adv. Mater.* **2014**, *26*, 7300.
[48] Y. Ji, C. Xiao, Q. Wang, J. Zhang, C. Li, Y. Wu, Z. Wei, X. Zhan, W. Hu, Z. Wang, R. A. J. Janssen, W. Li, *Adv. Mater.* **2016**, *28*, 943.
[49] D. Khim, Y. R. Cheon, Y. Xu, W.-T. Park, S.-K. Kwon, Y.-Y. Noh, Y.-H. Kim, *Chem. Mater.* **2016**, *28*, 2287.
[50] T. Lei, Y. Cao, X. Zhou, Y. Peng, J. Bian, J. Pei, *Chem. Mater.* **2012**, *24*, 1762.
[51] T. Lei, J.-H. Dou, J. Pei, *Adv. Mater.* **2012**, *24*, 6457.
[52] K. J. Fallon, N. Wijeyasinghe, E. F. Manley, S. D. Dimitrov, S. A. Yousaf, R. S. Ashraf, W. Duffy, A. A. Y. Guilbert, D. M. E. Freeman, M. Al-Hashimi, J. Nelson, J. R. Durrant, L. X. Chen, I. McCulloch, T. J. Marks, T. M. Clarke, T. D. Anthopoulos, H. Bronstein, *Chem. Mater.* **2016**, *28*, 8366.
[53] H. N. Tsao, K. Mullen, *Chem. Soc. Rev.* **2010**, *39*, 2372.
[54] D. I. James, S. Wang, W. Ma, S. Hedström, X. Meng, P. Persson, S. Fabiano, X. Crispin, M. R. Andersson, M. Berggren, E. Wang, *Adv. Electron. Mater.* **2016**, *2*, 1500313.
[55] Z. Mao, Y. Guo, H. Chen, W. Zhang, G. Yu, *Polymer* **2016**, *99*, 496.
[56] J. Yang, H. Wang, J. Chen, J. Huang, Y. Jiang, J. Zhang, L. Shi, Y. Sun, Z. Wei, G. Yu, Y. Guo, S. Wang, Y. Liu, *Adv. Mater.* **2017**, *29*, 1606162.
[57] S. Cho, J. Lee, M. Tong, J. H. Seo, C. Yang, *Adv. Funct. Mater.* **2011**, *21*, 1910.
[58] Z. Chen, M. J. Lee, R. Shahid Ashraf, Y. Gu, S. Albert-Seifried, M. Meedom Nielsen, B. Schroeder, T. D. Anthopoulos, M. Heeney, I. McCulloch, H. Sirringhaus, *Adv. Mater.* **2012**, *24*, 647.
[59] B. B.-Y. Hsu, C.-M. Cheng, C. Luo, S. N. Patel, C. Zhong, H. Sun, J. Sherman, B. H. Lee, L. Ying, M. Wang, G. Bazan, M. Chabinyc, J.-L. Brédas, A. Heeger, *Adv. Mater.* **2015**, *27*, 7759.
[60] C. Luo, A. K. K. Kyaw, L. A. Perez, S. Patel, M. Wang, B. Grimm, G. C. Bazan, E. J. Kramer, A. J. Heeger, *Nano Lett.* **2014**, *14*, 2764.
[61] R. Dovesi, R. Orlando, A. Erba, C. M. Zicovich-Wilson, B. Civalleri, S. Casassa, L. Maschio, M. Ferrabone, M. De La Pierre, P. D'Arco, Y. Noël, M. Causà, M. Rérat, B. Kirtman, *Int. J. Quantum Chem.* **2014**, *114*, 1287.